Millimeter-Wave Channel Characterization in Large Hall Scenario at the 10 and 28 GHz Bands

Zhang, Guojin; Hanpinitsak, Panawit ; Cai, Xuesong; Fan, Wei; Saito, Kentaro; Takada, Jun-ichi ; Pedersen, Gert Frølund

Published in:
13th European Conference on Antennas and Propagation (EuCAP)

Publication date:
2019

Document Version
Accepted author manuscript, peer reviewed version

Millimeter-Wave Channel Characterization in Large Hall Scenario at the 10 and 28 GHz Bands

Guojin Zhang[1], Panawit Hanpinitsak[2], Xuesong Cai[1], Wei Fan[1], Kentaro Saito[2], Jun-ichi Takada[2], and Gert Frølund Pedersen[1].

[1]Department of Electronic Systems, Section Antennas, Propagation and Millimetre-wave Systems (APMS), Aalborg University, Aalborg, 9220, Denmark.

[2]Department of Transdisciplinary Science and Engineering, School of Environment and Society, Tokyo Institute of Technology, Tokyo, Japan.

Email: [1]{guojin, xuc, wfa, gfp} @es.aau.dk, [2] {hanpinitsak.p@ap.ide.titech.ac.jp, saitouken@tse.ens.titech.ac.jp, takada@ide.titech.ac.jp.}

***Abstract*—This paper presents the characteristics of the mm-wave propagation channel in hall scenario at the frequency bands of 9−11 GHz and 27−29 GHz. The spherical propagation parameters, i.e. delay, azimuth, elevation, source distance and complex amplitude are estimated by the high resolution parameter estimation (HRPE) algorithm. Based on the results, the channel characteristics, e.g. path loss, delay spread, and angle spread are analyzed for different mm-wave bands. The results reveal that the line of sight and specular components are dominant in such large size scenario at 9−11 GHz and 27−29 GHz bands, and little differences in the characteristics between the two bands can be observed.**

***Index Terms*—Millimeter-wave, path loss, delay spread and angle spread.**

I. Introduction

The next generation communication system (5G) is moving towards frequency bands above 6 GHz, due to the plenty of available spectrum and higher data traffic supported at millimeter wave (mm-wave) bands. Accurate knowledge of the channel propagation characteristics in mm-wave frequencies band is important for mm-wave system design and performance evaluation [1].

Extensive measurement campaigns have been conducted for mm-wave channels, with focusing on the comparison of channels in different frequency bands in the same environment [2]–[4]. In [2], the measurements were conducted in a typical indoor office environment at 28 GHz and 73 GHz frequency bands. Large-scale path loss and temporal statistic are provided, using rotatable directional horn antennas. In [5], the frequency dependency of propagation parameters, e.g. power delay profile, delay spread, path loss and shadow fading were investigated in three different indoor environments, such as hall, meeting room and corridor scenarios. In [6], the large scale parameters, i.e. path-loss, shadowing, cross-polarization power ratio, delay spread and coherence bandwidth were investigated in various indoor environments at 11 GHz, including two hall scenarios and three rooms. To the author's best knowledge, the analysis of the channel characteristics at different frequency bands in these indoor cases, is still limited comparing the power spectrum and delay spread in most papers.

In this paper, the comparison of propagation characteristics with total 20 Tx antenna locations at 9−11 GHz and 27−29 GHz bands in large hall scenario are investigated. The high resolution parameter estimation (HRPE) algorithm is used for extracting the information of delay, angle and amplitude, which are used for calculating the characteristics, such as path loss, delay spread and angle spread.

The rest of this paper is organized as follows. In Section II, the measurement campaign is presented. Section III describes the channel characteristics, and the results of propagation parameters are analyzed. Section IV summarizes the conclusions.

II. Measurement campaign

Fig. 1 illustrates the top-view sketch of the hall scenario in Aalborg University, where the measurement campaign was conducted at the frequency band of 9−11 GHz and 27−29 GHz, using a channel sounder [3], [7] based on a vector network analyzer (VNA). The measurement setup parameters are depicted in Table I. The shape of the hall is irregular, with 39 m from west to east, 20 m from north to south and 10 m height from the ground to the ceiling. The four big yellow ventilation tubes and six small white pillars are located around the hall.

The commercial biconical antenna SZ-2003000/P [8] was used as transmitter (Tx) antenna and homemade biconical antenna [9] was used as receiver (Rx) antenna, as shown in Fig. 2. The Rx antenna was rotated clockwise on a rotating pedestal with a pre-set radius of 0.24 m with 1 degree rotating steps, to form a large-scale uniform circular array (UCA) with 360 elements. The antenna gains of commercial antenna are 2.75 dBi at 10 GHz and 4.8 dBi at 28 GHz. For the homemade antenna, the gains are 3.5 dBi at 10 GHz and 6 dBi at 28 GHz. A total of 20 spatial snapshots were measured by moving the Tx antenna and the Rx antenna was located near the yellow ventilation tubes as shown in Fig. 1. Each Tx in each row was spaced 1 m apart. The height of the Tx and Rx antennas is

TABLE I
MEASUREMENT SETUP.

Room	Hall
Dimension (m^3)	$39 \times 20 \times 10$
Tx antenna	Commercial biconical SZ-2003000/P
Rx antenna	Homemade biconical antenna
Center frequency	10, 28 GHz
Bandwidth	2 GHz
Tx\Rx antenna height	1.50 m
Frequency sweep points	360
Frequency samples	750
UCA radius	0.24 m

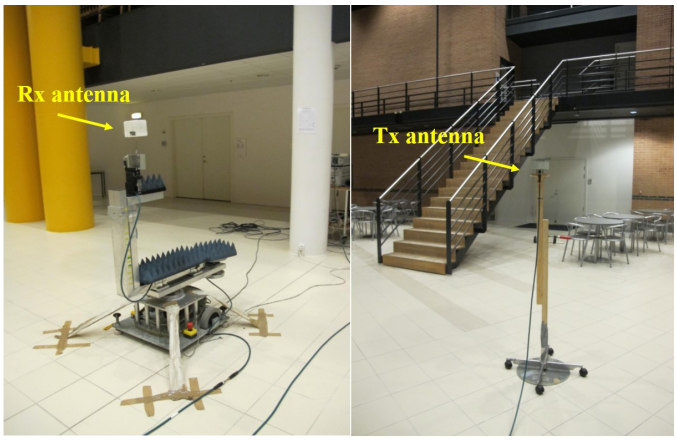

Fig. 2. The photograph of Rx (left) and Tx (right) antennas.

mounted at 1.50 m. The measurement was conducted with a bandwidth of 2 GHz and 750 samples were collected for each frequency band.

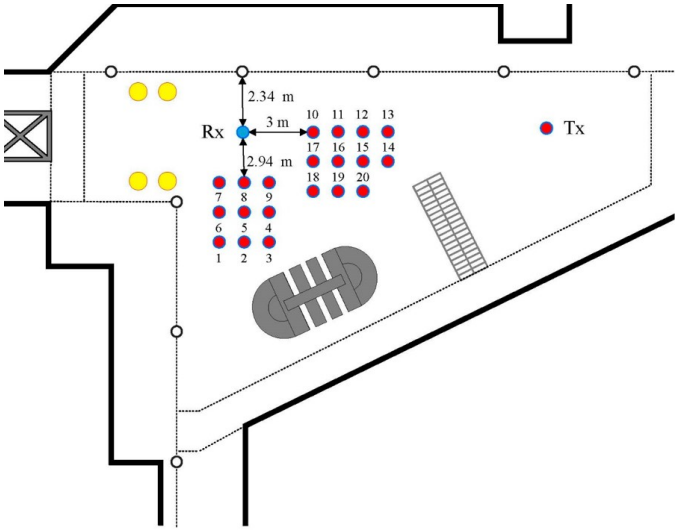

Fig. 1. Top view of the hall scenario with 20 Tx locations and single Rx location.

III. RADIO CHANNEL CHARACTERIZATION

The measured raw data is processed by the hanning window and inverse Fourier transform (IFT), then the average power delay profiles (APDPs), which can be obtained by the channel impulse response (CIR) $h_{m,n}(\tau)$ as

$$P_m(\tau) = \frac{1}{N}\sum_{n=1}^{N}|h_{m,n}(\tau)|^2 \tag{1}$$

where $h_{m,n}(\tau)$ represents the CIR at m-th delay sample and n-th measured element.

In order to study the channel characteristics of the mm-wave spherical propagation, the HRPE algorithm [10] is applied to derive the parameters of the UCA channels, i.e. azimuth angles, elevation angles, delays, source distances and amplitudes of multipath components (MPCs). The spatial-temporal CIR $h(t;\tau,\theta,\phi,d)$ can be described as

$$h(t;\tau,\theta,\phi,d) = \sum_{l=1}^{L}\alpha_l\delta(\tau-\tau_l)\delta(\theta-\theta_l)\delta(\phi-\phi_l)\delta(d-d_l), \tag{2}$$

where L is the number of spherical waves impinge into the UCA, α_l represents the complex amplitude, τ_l is the propagation delay, θ_l and ϕ_l represent the azimuth and elevation angles of the l-th path, respectively. d_l is the propagation distance between the UCA center and the last source point during the propagation route of the l-th path, respectively. These parameters are used for calculating the characteristics of the channel propagation in this section.

A. Path loss

Path Loss is a fundamental channel model for estimating the link budget and coverage in cellular network [11]. The path loss of each Tx location can be calculated by the sum power of the CIRs, which can be represented as

$$PL = P_{\mathrm{Tx}} - P_{\mathrm{Rx}} + G_{\mathrm{Tx}} + G_{\mathrm{Rx}}[\mathrm{dB}] \tag{3}$$

where P_{Tx} and P_{Rx} are the transmit and received power, respectively. G_{Tx} and G_{Rx} are the the gains of the Tx and Rx antennas used at the measurement frequency, respectively. The path loss can be represented by the integrating all the power of the paths, can be obtained by the CIRs as

$$P_{Tx} - P_{Rx} = \sum_{m=1}^{M} P_m(\tau) \tag{4}$$

Table II show the path loss model fitting results, in which the path loss model is expressed by

$$PL(d)[\mathrm{dB}] = a + 10\cdot b\log_{10}(d[\mathrm{m}]) + X_\sigma \tag{5}$$

where a is the fading constant and b is the path loss exponent, which are both the least-square fits of floating intercept and the

TABLE II
PATH LOSS MODEL PARAMETERS.

Frequency band (GHz)	a	b	X_σ
10	51.651	1.712	0.195
28	63.725	1.525	0.468

slope. d represents the distance between Tx and Rx antennas, with the reference distance set as 1 m. X_σ denotes the shadowing variation, which is represented by the log-normal random variable with standard deviation σ.

Fig. 3(a) shows the measured path loss compared with the free space path loss at the frequency bands of 9-11 GHz and 27-29 GHz. The measured path loss at 9-11 GHz is little lower than free space path loss. While, in case of 27-29 GHz band, the measured path loss was roughly the same as free space path loss. It can also be seen from the results in Table II that the path loss exponents b are similar to 2 due to large size of the hall scenario. These results match the results in [2] which reported that the b decreases with frequencies and values are higher than 1.5.

B. Delay Spread

The delay spread is widely used for characterizing the MPCs richness of the channels [12]. In this section, delay spread is calculated by two methods. The first method is based on the measured raw data with dynamic range of 25 dB, and the second is based on the delay information estimated by HPRE algorithm.

The delay spread is calculated as the second-order central moments of APDPs. The mean delay $\bar{\tau}$ and root mean square delay spread σ_τ with the first method can be computed as [12]

$$\bar{\tau} = \frac{\sum_{m=1}^{M} P_m(\tau) \cdot \tau}{\sum_{m=1}^{M} P_m(\tau)}, \tag{6}$$

$$\sigma_\tau = \sqrt{\frac{\sum_{m=1}^{M} P_m(\tau) \cdot \tau^2}{\sum_{m=1}^{M} P_m(\tau)} - \bar{\tau}^2}. \tag{7}$$

For the second method, $P_m(\tau)$ need to be replaced by the square of complex amplitude $|\alpha_l|^2$ obtained by the HPRE algorithm. Besides that, the delay sample m and M should be exchanged with the number of the estimated paths l and L, respectively.

The similar trend by the two methods at 10 GHz and 28 GHz can be observed from Fig. 3(b). The difference between the two methods at the same frequency is due to the affect of the sidelobes in measured raw data. Thus, more accurate results can be achieved by the HPRE algorithm. The lowest values of delay spread can be seen at position 7-10 and 17-18, where is the smallest Tx-Rx distance.

C. Angle Spread

Because the estimated elevation angles are almost close to 90 degrees, only azimuth angles are investigated. The angle spread σ_θ can be calculated, as defined in [10], [13],

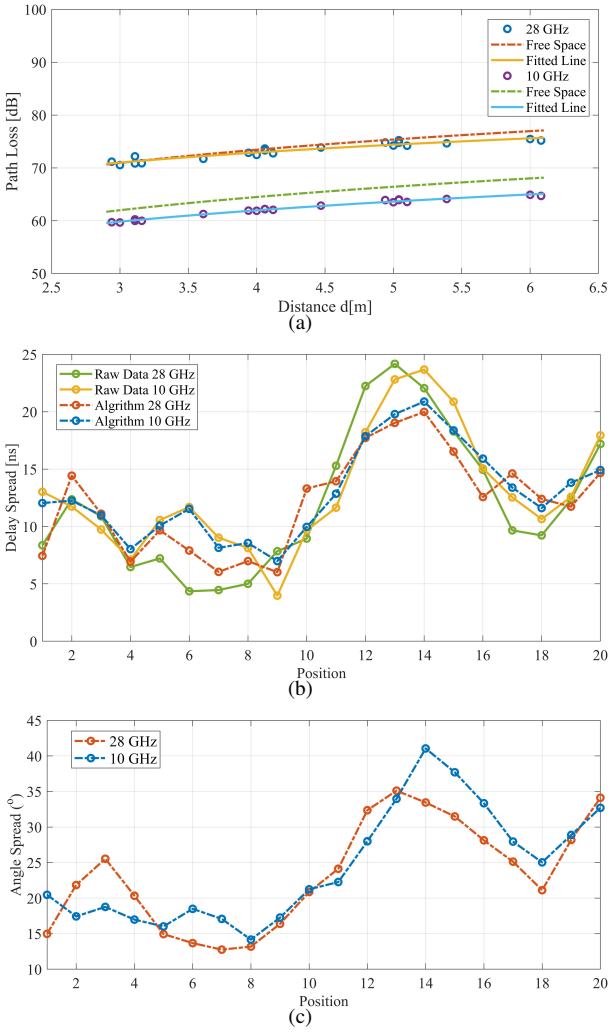

Fig. 3. The channel characteristics in hall scenario at total 20 Tx locations. (a) Path Loss. (b) Delay Spread. (c) Angle Spread.

$$\sigma_\theta = \sqrt{-2\log\left(\left|\frac{\sum_{l=1}^{L} \exp(j\theta_l) \cdot |\alpha_l|^2}{\sum_{l=1}^{L} |\alpha_l|^2}\right|\right)}. \tag{8}$$

The large deviation in the values of angle spread is depicted in Fig. 3(c) at positions 5-10 and 12-16, 20. That is because positions 5-10 are much close to the Rx antenna, yellow ventilation tubes and pillars, the strong reflections at these positions are mainly from the white pillars and yellow ventilation tubes nearby with small range of azimuth. While positions 12-16 and 20 are relatively far from the Rx antenna, yellow ventilation tubes and pillars, the reflections are mainly from the walls around with large range of azimuth.

According to the power angle delay profiles (PADPs) of position 8 obtained by the HRPE algorithm in Fig. 4(a), the main specular components after the LOS path are identified and plotted in Fig. 4(b). It could be seen that strong specular reflected paths are mainly contributed by the yellow ventilation tubes and white pillars. On the other hand, the main specular

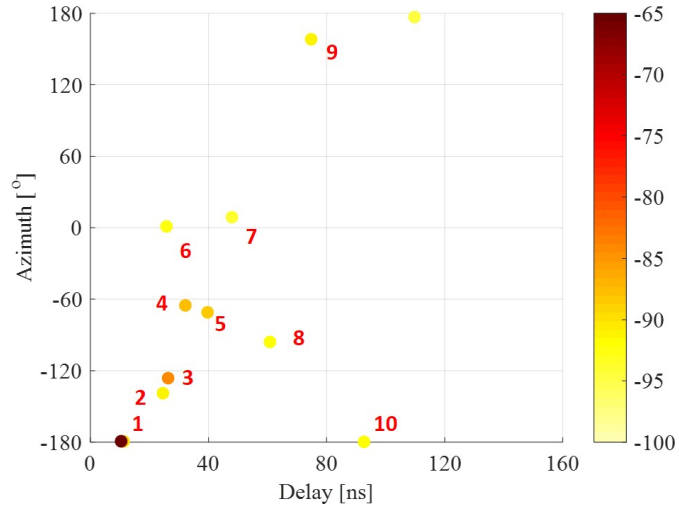

(a)

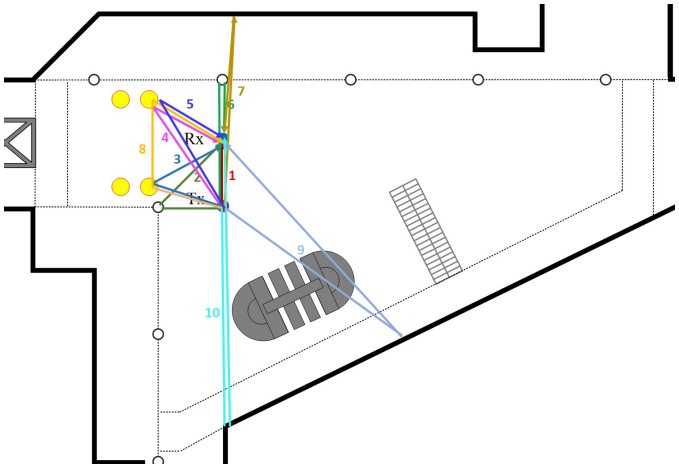

(b)

Fig. 4. The PADPs and identified paths of Tx positions 8 at 27 GHz-29 GHz in Hall.

components after the LOS path are sparse at 10 and 28 GHz bands and the LOS components are dominant at the positions with small Tx-Rx distance.

IV. Conclusion

In this paper, the radio channel of hall scenario is characterized at frequency bands of 9−11 GHz and 27−29 GHz. Based on the virtual uniform circular array (UCA) system and high resolution parameter estimation (HRPE) algorithm, specular propagation paths are identified and their delay, azimuth and elevation information are estimated. The properties of the radio channel at 9−11 GHz and 27−29 GHz bands are studied in terms of path loss, angle spread, and delay spread. The result shows that the differences between two frequency bands are mostly minor. The measured path loss at 27−29 GHz is similar with the free space path loss, duo to dominant LOS path. The path loss exponents b are higher than 1.5 at 9−11 GHz and 27−29 GHz, due to the large size of the hall scenario. It can also be observed that the values of delay spread obtained by HRPE algorithm are more accurate than that by measured raw data, with the range of 6−20 ns. The values of angle spread are mainly ranged between 12.75 ° and 41 °. In order to reveal further channel characteristics in non-line of sight scenarios, more measurements and simulation data are still needed.

References

[1] T. S. Rappaport, S. Sun, R. Mayzus, H. Zhao, Y. Azar, K. Wang, G. N. Wong, J. K. Schulz, M. Samimi, and F. Gutierrez, "Millimeter wave mobile communications for 5G cellular: It will work!" *IEEE Access*, vol. 1, pp. 335–349, 2013.

[2] G. R. Maccartney, T. S. Rappaport, S. Sun, and S. Deng, "Indoor office wideband millimeter-wave propagation measurements and channel models at 28 and 73 GHz for ultra-dense 5G wireless networks," *IEEE Access*, vol. 3, pp. 2388–2424, 2015.

[3] W. Fan, I. Carton, J. Ø. Nielsen, K. Olesen, and G. F. Pedersen, "Measured wideband characteristics of indoor channels at centimetric and millimetric bands," *EURASIP Journal on Wireless Communications and Networking*, vol. 2016, no. 1, p. 58, Feb 2016. [Online]. Available: https://doi.org/10.1186/s13638-016-0548-x

[4] J. Vehmas, J. Jarvelainen, S. L. H. Nguyen, R. Naderpour, and K. Haneda, "Millimeter-wave channel characterization at helsinki airport in the 15, 28, and 60 GHz bands," in *2016 IEEE 84th Vehicular Technology Conference (VTC-Fall)*, Sept 2016, pp. 1–5.

[5] S. Geng and P. Vainikainen, "Frequency and bandwidth dependency of UWB propagation channels," in *2006 IEEE 17th International Symposium on Personal, Indoor and Mobile Radio Communications*, Sept 2006, pp. 1–5.

[6] M. Kim, Y. Konishi, Y. Chang, and J. Takada, "Large scale parameters and double-directional characterization of indoor wideband radio multipath channels at 11 GHz," *IEEE Transactions on Antennas and Propagation*, vol. 62, no. 1, pp. 430–441, Jan 2014.

[7] P. Hanpinitsak, K. Saito, W. Fan, J.-i. Takada, and G. F. Pedersen, "Frequency characteristics of path loss and delay-angular profile of propagation channels in an indoor room environment in SHF bands," in *Mobile Communication Workshop*, 2017.

[8] ainfoinc, "SZ-2003000-P.pdf [online]." Available: http://www.ainfoinc.com/en/pro_ pdf/new_ products/antenna/Bi-Conical%20Antenna/tr_ SZ-2003000-P.pdf, Tech. Rep., (2018, June 5).

[9] S. S. Zhekov, A. Tatomirescu, and G. F. Pedersen, "Antenna for ultra-wideband channel sounding," *IEEE Antennas and Wireless Propagation Letters*, vol. 16, pp. 692–695, 2017.

[10] X. Cai and W. Fan, "A complexity-effcient high resolution propagation parameter estimation algorithm for ultra-wideband large-scale uniform circular array," *submitted to IEEE Trans. Commun.*, 2018.

[11] J. Ko, Y. Cho, S. Hur, T. Kim, J. Park, A. F. Molisch, K. Haneda, M. Peter, D. Park, and D. Cho, "Millimeter-wave channel measurements and analysis for statistical spatial channel model in in-building and urban environments at 28 GHz," *IEEE Transactions on Wireless Communications*, vol. 16, no. 9, pp. 5853–5868, Sept 2017.

[12] X. Cai, X. Yin, X. Cheng, and A. P. Yuste, "An empirical random-cluster model for subway channels based on passive measurements in UMTS," *IEEE Trans. Commun.*, vol. 64, no. 8, pp. 3563–3575, Aug 2016.

[13] 3GPP, "Study on channel model for frequencies from 0.5 to 100 GHz," *(3GPP TR 38.901 version 14.0.0 Release 14)*, 2018.